

Optical Communications through Atmospheric Turbulence Using Photodetector Arrays

Victor Vilnrotter and Meera Srinivasan

Jet Propulsion Laboratory, California Institute of Technology
4800 Oak Grove Dr., Pasadena, CA 91109-8099

ABSTRACT

Ground-based reception of optical signals from space suffers from degradation of the optical phase-front caused by atmospheric turbulence, leading to a reduction in the effective diameter of the receiving aperture and to random fluctuations of the point spread function in the focal plane. A proportional increase in the receiver's field of view, required to collect all of the signal, also causes a corresponding increase in the amount of interfering background radiation, resulting in degraded communications performance. These problems may be mitigated through the use of an optical detector array assembly in the focal plane that can adaptively select areas of higher signal density while ignoring areas predominated by background noise. This concept is investigated for both Poisson photon counting detector arrays and avalanche photodiode arrays. Kolmogorov phase screen simulations are used to model the sample functions of the focal-plane signal distribution due to turbulence and to generate realistic spatial distributions of the received optical field. The optimum photon counting array detector is derived and approximated by a simpler suboptimum structure that replaces the continuous weighting function of the optimal receiver by a hard decision on the selection of the signal detector elements. It is shown that for photon counting receivers observing Poisson distributed signals, performance improvements of up to 5 dB can be obtained over conventional single detector photon counting receivers, when observing turbulent optical fields in high background environments. For the avalanche photodiode detector case, it is shown that gains of up to 4 dB may be achieved by using the array receiver rather than a single APD, but that a photon-counting array still performs about 5.5 dB better than an APD array.

1. INTRODUCTION

Ground-based reception of optical signals from space suffers from degradation of the optical phase-front caused by atmospheric turbulence. This leads to a reduction in the effective diameter of the receiving aperture, and to random fluctuations of the receiver's "point spread function" (PSF) in the focal plane. For example, the diffraction-limited field-of-view (FOV) of the receiving telescope (with collecting diameter D_R at wavelength λ) can be taken to be approximately $\theta_{dl} \cong \lambda / D_R$ which, for a 3 meter aperture and one micron wavelength translates to 0.33 microradians. If the effective focal length of the telescope is 6 meters (implying an F/2 receiver), then a diffraction-limited PSF of 2 micron diameter, or 0.002 mm, will be produced in the focal-plane. Thus, under ideal conditions a very small detector could be used to collect virtually all of the signal energy, while at the same time spatially filtering out most of the background radiation. However, atmospheric conditions rarely permit diffraction-limited operation of large telescopes: even under "good" nighttime seeing conditions, the phase of the received signal field tends to become uncorrelated over distances greater than 20 cm, deteriorating to as little as 2-4 cm during the day [1]. Under these conditions, the dimensions of the PSF in the focal-plane tends to increase inversely with coherence length, as if the dimensions of a diffraction-limited telescope were correspondingly reduced: the telescope still collects all of the signal energy propagating through its physical aperture, but the collected signal energy is re-distributed into a much larger spot in the focal-plane. Thus, the receiver's FOV must be increased proportionally to collect the signal, leading to a corresponding increase in the amount of interfering background radiation collected by the receiver.

An example of the increase in the effective dimensions of the receiver's point-spread function over its diffraction-limited value is shown in the contour plot of Figure 1, obtained from a Kolmogorov phase screen simulation of a 1m telescope aperture with 0.3m central obstruction, and 4cm atmospheric coherence length. For this example, the dimensions of the diffraction-limited PSF correspond to a single pixel of the 16X16 square array superimposed over the signal distribution, illustrating the increase in the effective PSF produced by turbulence.

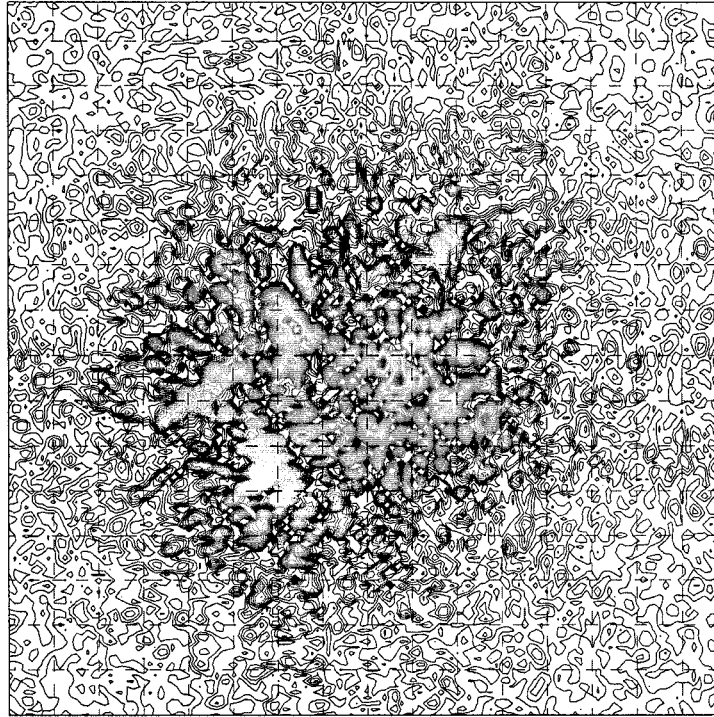


Figure 1. Contour plot of instantaneous focal-plane signal distribution (covering 16X16 detector array) due to atmospheric turbulence: 4 cm coherence length, 45X45 microradian FOV.

In order to collect all of the signal energy, the dimensions of a single optical detector must be made large enough to encompass the degraded point-spread function as well as its random excursions in the focal-plane, which tend to change on time-scales of 10-100 msec. However, a large detector implies a large receiver field-of-view, which in turn implies a corresponding increase in the amount of background radiation admitted into the receiver. That, in turn, degrades communications performance. These problems are effectively mitigated by the use of a high-speed photon-counting detector array in conjunction with high-speed digital electronics capable of performing the signal-processing functions required for optimum or near-optimum receiver performance.

2. OPTICAL DIRECT DETECTION WITH FOCAL-PLANE ARRAYS

In the following analysis we assume that a “multimode” assumption can be applied to the background fields. It has been shown that multimode Gaussian fields with suitably small average modal noise count generate approximately Poisson distributed random point processes at the output of an ideal “photon-counting” detector [2]. Since coherent fields generated by a laser are also conditionally Poisson, this model justifies the use of the Poisson model for both signal and background radiation which, in turn, leads to mathematically tractable solutions.

2.1 Single detector model

Suppose that a single detector element “measures” the number of photons contained in the received field by producing a stream of electrons at its output terminal in response to the absorbed photons. If each electron gives rise to a pulse, and if the amplitude of each pulse is normalized to unity, then we can define a “count record” consisting of positive integer-valued

jumps occurring each time a photon is detected [3]. Given a particular realization of the intensity function, $\lambda(t)$, the joint density of occurrence times conditioned on the number of absorbed photons N and on the intensity function $\lambda(t)$, is given by

$$p(\mathbf{w} | N, \lambda(t)) = \frac{p(\mathbf{w}, N | \lambda(t))}{p(N | \lambda(t))} = (N!) \prod_{i=1}^N \lambda(w_i) \left(\int_0^T \lambda(t) dt \right)^{-1} \quad (1)$$

where $\mathbf{w} = (w_1, w_2, \dots, w_N)$ is the set of occurrence times of the absorbed photons. This expression describes the output of a single ‘‘photon counting’’ detector responding to optical intensity. If instead of just a single detector, an array of detectors were used to detect the optical fields, the notation must be suitably generalized to enable unambiguous description of the output of each detector element.

2.2 Array detector model

Consider a rectangular array of detectors consisting of KXL detector elements. For some applications, such as finding the ‘‘center’’ of the signal intensity distribution, it is important to know the location of each detector element within the array; therefore, we include the subscripts mn , $1 \leq m \leq K$, $1 \leq n \leq L$, to denote the position of the detector element within the array. Thus, the sample function density defined in (1) can be written as $p[N_{mn}(t) | \lambda_{mn}(t); 0 \leq t < T]$ which now represents the output of a particular element of the array. Note that $\lambda_{mn}(t)$ can be viewed as that portion of a spatially distributed intensity function intercepted by the mn -th detector element. Note that if the spatial intensity distribution is known, and the location and size of each detector element is also known, then conditioning on the spatial intensity distribution is equivalent to conditioning on the array of intensity components, each of which is still a function of time. Assuming that each array element observes the sum of a signal-field plus multimode Gaussian noise-field with average noise-count per mode much less than one, the array outputs can be modeled as conditionally independent Poisson processes, conditioned on the average signal intensity over each detector element [2, 4]. Hence we denote the joint conditional sample function density of the array as

$$p[\mathbf{N}(t) | \lambda(t); 0 \leq t \leq T] = \prod_{m=1}^K \prod_{n=1}^L p[N_{mn}(t) | \lambda_{mn}(t); 0 \leq t < T] \quad (2)$$

where $\mathbf{N}(t) \equiv (N_{11}(t), N_{12}(t), \dots, N_{KL}(t))$, and each component on the right-hand-side of (2) is of the form defined in (1). This can be used as a starting point for problems involving hypothesis testing and parameter estimation, where the desired information is contained in the intensity distribution but only the array of count accumulator functions can be observed.

2.3 Hypothesis testing for Poisson processes

Consider M -ary pulse-position modulation (PPM) in which one of M intensity functions is received, and the receiver attempts to determine the correct symbol based on observations of the array of count accumulator functions over each of M time slots. It is assumed that the symbol boundaries are known, and that the arrival time of each detected photon and the total number of detected photons can be stored for a limited duration of time necessary for processing. With M -ary PPM modulation, a signal pulse of duration τ seconds is transmitted in one of M consecutive time-slots, resulting in a PPM symbol of duration $T = \tau M$ seconds. After propagating through the atmosphere and through the receiving optics, this temporal intensity function is transformed into a space-time intensity function in the detector-plane. The receiver also collects background energy from all directions, which is assumed to contribute an additional constant intensity of λ_b per detector element. The integrated intensity over the mn -th detector element is designated as $\lambda^{(i)}_{mn}(t)$, where the superscript refers to the i -th hypothesis. Suppose that each of the M messages is equally likely to be transmitted with probability M^{-1} , and that each message generates a unique vector of detector array intensities at the receiver, denoted by

$\lambda^{(i)}(t) = (\lambda_{i1}^{(i)}(t), \lambda_{i2}^{(i)}(t), \dots, \lambda_{iKL}^{(i)}(t))$. At the end of T seconds, the post-detection processor computes the probability of having received the observed array of count accumulator functions, and selects that message corresponding to the greatest probability of having been received. As shown in [4], the decoder selects the message corresponding to the greatest “log-likelihood” function, $\Lambda_i(T)$, evaluated after T seconds and conditioned upon the signal occurring in the i -th time-slot:

$$\Lambda_i(T) = \sum_{m=1}^K \sum_{n=1}^L \left\{ \sum_{w_{j,mn} \in ((i-1)\tau, i\tau]} \ln \left(1 + \frac{\lambda_{s,mn}(w_{j,mn})}{\lambda_b} \right) \right\} = \sum_{m=1}^K \sum_{n=1}^L \ln \left(1 + \frac{\lambda_{s,mn}}{\lambda_b} \right) N_{mn}^{(i)} \quad (3)$$

where $N_{mn}^{(i)}$ is defined as the total number of photons occurring over the mn -th detector element during the i -th time-slot, and $w_{j,mn}$ is the occurrence time of the j -th photon over the mn -th detector element within the same time-slot. Note that with constant signal intensities the actual arrival-times of photons within each slot do not contribute to the decision, hence only the total number of detected photons, $N_{mn}^{(i)}$, matters. Given that we know the intensity over each detector element, the i -th log-likelihood function consists of the sum of a logarithmic function of the ratio of signal and background count intensities from all detector elements over the i -th pulse-interval, multiplied by the total number of detected photons. The optimum detection strategy is to select the symbol corresponding to the greatest resulting log-likelihood function.

2.4 Performance of the optimum detector-array receiver

The probability of a correct decision is just the probability that the log-likelihood function associated with the transmitted symbol exceeds all other log-likelihood functions. Thus, when the q -th symbol was sent, a correct decision is made if $\Lambda_q(T) > \Lambda_i(T)$ for all $i \neq q$. Denoting the logarithmic functions, or “weights”, in (3) by u_{mn} , the log-likelihood function can be rewritten as

$$\Lambda_i(T) = \sum_{m=1}^K \sum_{n=1}^L u_{mn} N_{mn}^{(i)} \quad (4)$$

In this form, we can see that the log likelihood function is composed of sums of a random number of weights from each detector element: for example, the mn -th detector element contributes an integer number of its own weight to the sum. The probability density of the log likelihood function is the convolution of the probability densities from each detector element, and therefore all possible combinations of sums are represented. If hypothesis “ q ” is true, denoted by H_q , then the intensity in the q -th slot contains both signal and background energy, whereas the intensities in all other slots contain background energy only.

The received symbol is decoded correctly if the sum of weights from all detector elements over the signal-slot exceed the sum of weights from every other (non-signal) slot. However, since the weights for each log-likelihood function are the same, it is possible that the same maximum sum occurs over two or more slots, one of which is the true signal-slot, thus creating a “tie for biggest”. This tie is optimally resolved by a random choice among the biggest likelihood functions. Define the set of ordered numbers over which the probability density of the i -th log likelihood function takes on values as $\{\alpha_0 = 0, \alpha_1, \alpha_2, \dots\}$ and let $\Pr[\Lambda_i(T) = \alpha_k | H_q] \equiv p_i(\alpha_k | H_q)$. Taking all cases into account and assuming equiprobable signals, the probability of correctly decoding the received symbol is

$$P_M(C) = P_M(C | H_q) = \left\{ \sum_{r=0}^{M-1} \left(\frac{1}{r+1} \right) \binom{M-1}{r} \sum_{k=1}^{\infty} P_q(\alpha_k | H_q) [p_i(\alpha_k | H_q)]^r \left[\sum_{j=0}^{k-1} p_i(\alpha_j | H_q) \right]^{M-1-r} \right\} + M^{-1} \left\{ p_q(\alpha_0 | H_q) [p_i(\alpha_0 | H_q)]^{M-1} \right\} \quad (5)$$

where $p_q(-)$ and $p_i(-)$, $i \neq q$, refer to the probability densities corresponding to the signal and null hypotheses, respectively. The probability of a symbol error is $P_M(E) = 1 - P_M(C)$. When the array consists of a single detector, the weights can be set to one, and the probabilities are then governed by the Poisson density defined over the integers. Note that by counting all ties as errors in equation (5) a lower bound on the probability of correct detection, $P_M^l(C)$, is obtained that is much easier to compute, namely

$$P_M(C) \geq P_M^l(C) \equiv \sum_{k=1}^{\infty} p_q(\alpha_k | H_q) \left[\sum_{\substack{j=0 \\ i \neq q}}^{k-1} p_i(\alpha_j | H_q) \right]^{M-1} + M^{-1} \left\{ p_q(\alpha_0 | H_q) [p_i(\alpha_0 | H_q)]^{M-1} \right\} \quad (6)$$

This lower bound on the probability of correct detection yields the following useful upper bound on the error probability:

$$P_M^u(E) \equiv 1 - P_M^l(C) \geq P_M(E) \quad (7)$$

This upper bound will be evaluated in the following sections for several cases of interest.

2.5 The ‘‘Adaptive Synthesized Detector’’ Receiver

We observe from the preceding analysis that detectors containing much more background than signal intensity do not contribute significantly to the error probability, since the output of these detector elements are multiplied by weights that are close to zero. This observation suggests the following suboptimum decoder concept with greatly simplified structure: list the detector elements starting with the one containing the most signal energy, followed by every other detector ordered according to decreasing signal intensity. Compute the probability of error for the first detector element plus background, then form the sum of signal energies from the first two detector elements (plus background for two detector elements), and so on, until the minimum error probability is reached. Each set of detectors may be considered to be a single detector, so that no weighting is applied to account for variations in the signal distribution over the detector elements included in that set. The set of detector elements that achieves the minimum probability of error is the best ‘‘synthesized single detector’’ matched to the signal intensity distribution.

For the ‘‘adaptive synthesized single detector’’, the observed counts are modeled as Poisson random variables. For this case, the probability of correct decision is

$$P_M(C) = \left\{ \sum_{r=0}^{M-1} \left(\frac{1}{r+1} \right) \binom{M-1}{r} \sum_{k=1}^{\infty} \frac{(\lambda_s \tau + \lambda_b \tau)^k}{k!} e^{-(\lambda_s \tau + \lambda_b \tau)} \left[\frac{(\lambda_b \tau)^k}{k!} e^{-\lambda_b \tau} \right]^r \left[\sum_{j=0}^{k-1} \frac{(\lambda_b \tau)^j}{j!} e^{-\lambda_b \tau} \right]^{M-1-r} \right\} + M^{-1} e^{-(\lambda_s + M\lambda_b)\tau} \quad (8)$$

where the error probability is again given by $P_M(E) = 1 - P_M(C)$.

2.6 The Gaussian Approximation

When the array contains a large number of detector elements, the computation of the probability density of the weighted sum of Poisson random variables becomes prohibitively difficult. In that case, approximating the true discrete density with a simpler continuous density would be of great value. It is shown in [4] that a useful Gaussian approximation to the discrete density of the weighted sum of Poisson random variables can indeed be derived from the characteristic function of the discrete density, where the mean and variance of the approximating continuous random variable are set equal to the mean and variance of the weighted Poisson random variables. Assuming equal a-priori symbol probabilities, the probability of correctly decoding the received PPM symbol is again the probability that the random variable in the ‘‘signal plus noise’’ time-slot exceeds all of the other random variables in the remaining $(M - 1)$ ‘‘noise only’’ time slots (we need not consider

equalities here, since with continuous random variables equality is a zero-probability event). Recalling that the average intensity in the signal slot is $(\lambda_{s,mm} + \lambda_b)\tau$ while in all of the other slots it is $\lambda_b \tau$, and defining the mean and variance associated with signal and noise slots as η_{sb}, σ_{sb}^2 , and η_b, σ_b^2 , respectively, the probability of symbol error can be put into the form

$$P_M(E) = 1 - P_M(C) \cong 1 - \int_{-\infty}^{\infty} dy \frac{e^{-y^2/2}}{\sqrt{2\pi}} \left\{ 1 - \frac{1}{2} \text{Erfc} \left(\frac{\sigma_{sb}}{\sigma_b} y + \frac{\eta_{sb} - \eta_b}{\sigma_b} \right) \right\}^{(M-1)} \quad (9)$$

where Erfc is the complementary error function defined as $\text{Erfc}(x) = \frac{1}{\sqrt{2\pi}} \int_x^{\infty} e^{-y^2/2} dy$.

2.7 Performance bounds for Poisson detection

For the special case of binary *PPM*, the following useful upper bound has been obtained [4]:

$$P_2(E) \leq \exp(-\Delta^2) \left\{ \sum_{k=0}^{\infty} \left(\frac{\sqrt{\lambda_b \tau}}{\Delta + \sqrt{\lambda_b \tau}} \right)^k - \frac{1}{2} \right\} F_0(\psi) = \exp(-\Delta^2) \left(\frac{\sqrt{\lambda_b \tau}}{\Delta} + \frac{1}{2} \right) F_0(\psi) \equiv P_2(UB) \quad (10)$$

where $\Delta = \sqrt{(\lambda_s + \lambda_b)\tau} - \sqrt{\lambda_b \tau}$, $\psi = 2\tau \sqrt{(\lambda_s + \lambda_b)\lambda_b}$, and $F_k(\psi) = e^{-\psi} I_k(\psi)$, and where $I_k(\psi)$ is the modified Bessel function of order k . This upper bound on the binary *PPM* error probability can be further approximated in the limit of very small and very large background energies as

$$P_2(UB) \cong \begin{cases} \frac{1}{2} \exp(-\Delta^2) & \lambda_b \tau \ll 1 \\ \left(\frac{\sqrt{\lambda_b \tau}}{\Delta} + \frac{1}{2} \right) \frac{\exp(-\Delta^2)}{\sqrt{2\pi\psi}} & \lambda_b \tau \gg 1 \end{cases} \quad (11)$$

The upper bound on the binary *PPM* error probability can also be used to further bound *M*-ary *PPM* performance for the single detector case, in a manner similar to the ‘‘union bound’’ familiar from the ‘‘additive Gaussian noise’’ problem. The result is an expression of the form $P_M(E) \leq (M-1)P_2(E)$. The proof, presented in [7, Appendix B], is somewhat complicated by the fact that for the optical problem the probability of committing an error when attempting to resolve ties among maximal counts must also be taken into account.

3. NUMERICAL RESULTS

Performance comparison of the optimally weighted array receiver and the ‘‘adaptive synthesized single detector’’ receiver (also referred to as the ‘‘0-1’’ subarray in the figures) has been carried out for average background energies of $K_b \equiv \lambda_b \tau = 0.1$ and 1.0. Two different signal models were used: a simple ‘‘test’’ model where only five of the $16 \times 16 = 256$ total detector elements were assumed to contain signal energy while the rest were assumed to contain no signal, and a more realistic 16×16 detector array model where the signal distribution over the array was simulated using a Kolmogorov turbulence model as described in [8], and where all 256 detector elements may contain some signal.

For the test model the proportions of the total average absorbed signal energy $K_s \equiv \lambda_s \tau$ over the five detector elements were assumed to be (1.0, 0.3, 0.2, 0.05, 0.02). The results are shown in Figure 2 as a function of the total average absorbed signal

energy K_s . It is evident that optimal weighting (represented by large squares) yields somewhat better performance than the suboptimum "0-1 subarray": however, the improvements due to the significantly more complicated optimally weighted array are only about 0.3 dB at an error probability of 0.001 for the high background case.

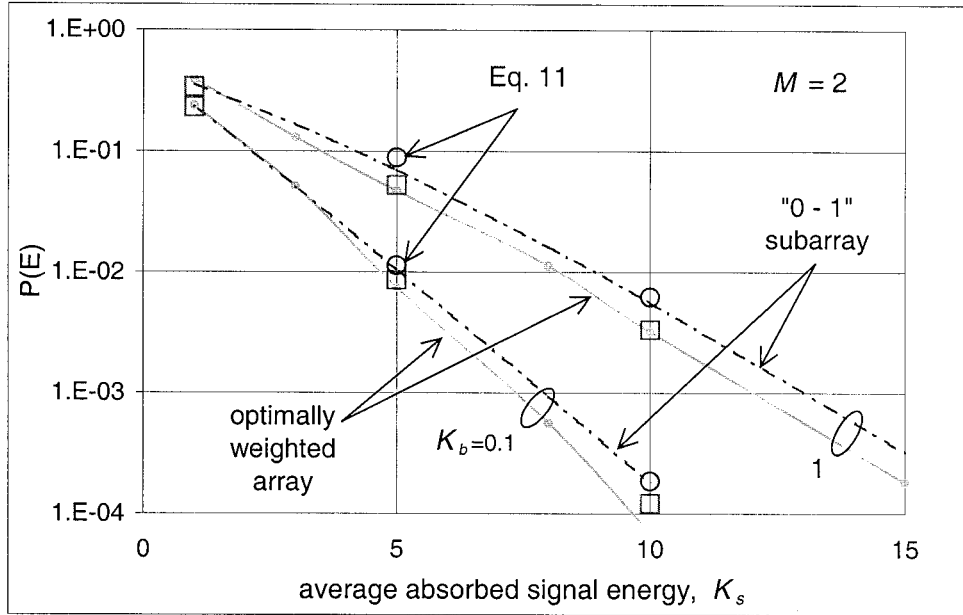


Figure 2. Exact error probabilities, Gaussian approximation to the weighted sum, and simulation results

The reason for using only five detectors in the examples of Figure 2 is that convolving more than five weighted Poisson densities rapidly becomes prohibitively difficult, due to excessive demands on computer memory. Therefore, only this "five-detector" example could be evaluated computationally through the use of the bound on the probability of correct detection defined in equation (6), and only for background intensities not exceeding an average of 2 photons per detector per slot.

In order to describe the spatial distribution of the signal in the detector plane, a sample field was generated using a "Kolmogorov phase-screen" program [8], resulting in a matrix of complex signal amplitudes. For the simulation, an atmospheric correlation length of $r_0 = 4$ cm was assumed, which implies that the results should apply to any receiving aperture that is much greater than this correlation length [1]. The field intensity generated in the detector plane by the simulation was then integrated over the elements of a 16X16 detector array which is assumed to encompass the extent of the signal distribution in the detector plane. The detector signal intensities are normalized so that for the mn -th detector we obtain an average number of absorbed signal photons of $\lambda_{s,mn}\tau$. Constant average background photon energy of $\lambda_b\tau$ is assumed over each detector element.

In Figure 3, a realistic spatial distribution of the signal intensity over the focal-plane was generated using Kolmogorov phase-screens. Monte-Carlo simulations were performed to evaluate the error probability for the optimally weighted array. The "Gaussian" approximation to the error probability has also been evaluated for the binary PPM case, with average background energies (per detector element) equal to 0.1, 1, and 5 photons/time-slot, as a function of the total average signal energy. It can be seen that the Gaussian approximation is close to the exact values obtained from Monte-Carlo simulation, and that good agreement is obtained even for small background energies per detector element, as direct comparison with the simulation results (large diamonds) indicates. In fact, it appears that this Gaussian approximation provides useful results over the entire range of background and signal energies represented in Figure 3. The performance of the "0-1" subarray is also shown as the dashed curves: as expected, its performance is somewhat worse than that of the optimally weighted array, but not significantly so.

Performance improvements were also obtained for several different focal-plane distributions at an average background energy of one photon per detector per slot, to verify that the above results were typical. Only one of the phase-screen simulations yielded an unusually favorable signal distribution that achieved optimum performance with only 4 detector elements, but still needed roughly 22 signal photons for 0.001 error probability.

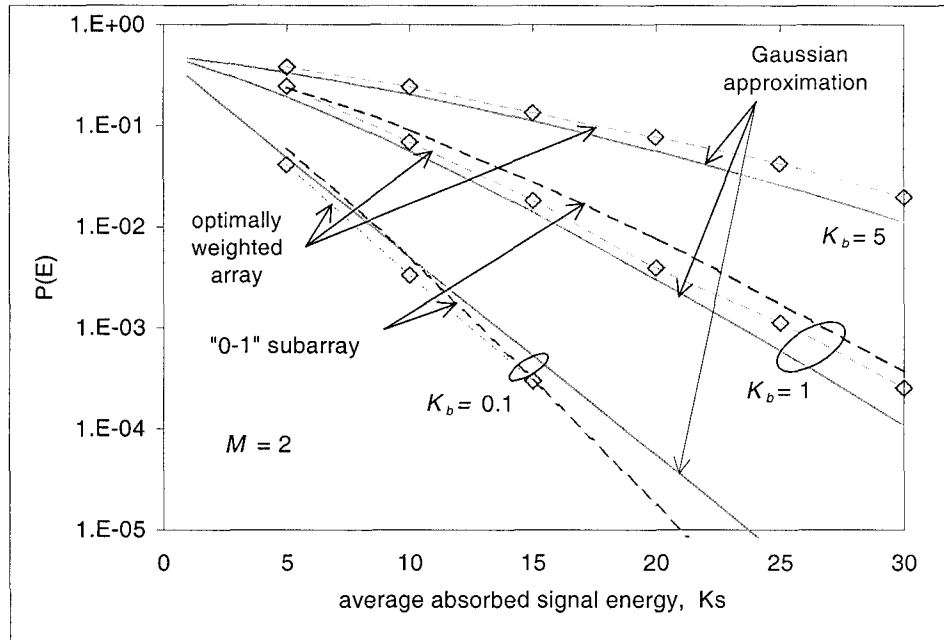


Figure 3. Exact error probabilities, Gaussian approximations to the weighted sum, and simulation results.

We can conclude, therefore, that for different distributions generated using the same atmospheric and receiver parameters similar receiver performance is obtained, justifying the use of a “representative” signal distribution for the numerical analysis.

In Figures 4a and 4b, *PPM* symbol error probabilities are shown as a function of the total average number of absorbed signal photons for the cases discussed above. In Figure 4a, binary error probabilities were computed for an average background photon count of 1.0 photon/detector/slot, indicating performance gains by the “adaptive synthesized single detector” over a single “large” non-adaptive detector of 2.8 at an error probability of 0.001, corresponding to 4.5 dB of performance improvement. Note the excellent agreement of the approximation of equation (11) (large circles) with the computed values. When compared to the ideal “adaptive optics” receiver that concentrates all of the collected signal energy in a single element of the array, the gain is 8.2, corresponding to 9.1 dB of improvement. Note that the optimally weighted array yields only about 0.3 dB improvement over the optimized “0-1” subarray at a symbol error probability of 0.001, even with the relatively high background energy of $K_b = 1$. Similar gains are evident in Figure 4b, which represent the symbol error probability, $P(SE)$, of the optimized subarray observing 16-dimensional ($M = 16$) *PPM*. The accuracy of the “union bound” evaluated for the case $\lambda_b \tau \gg 1$ is evident (large circles), especially at the lower error probabilities.

In Figures 5a and 5b we show performance of the optimized “0-1” subarray and single large non-adaptive detector when avalanche photodiode detectors with follow-on amplifiers are used instead of photon counting detectors, as described in [10]. The output of APD’s differs substantially from that of photon counting detectors and is distributed as the sum of Webb and Gaussian random variables, but modeled here as a purely Gaussian process with mean and variance parameters as given in [10]. Figures 5a and 5b show typical APD array results for $M = 2$ and $M = 16$, respectively, when $K_b = 1$. We see from these figures that APD array detection gains approximately 4 dB over detection with a single large APD at symbol error probability 0.001. While significant, these gains are smaller than those achievable through the use of photon-counting arrays. Figures 5a and 5b also show photon-counting array results, which are about 5.5 dB better than APD array results.

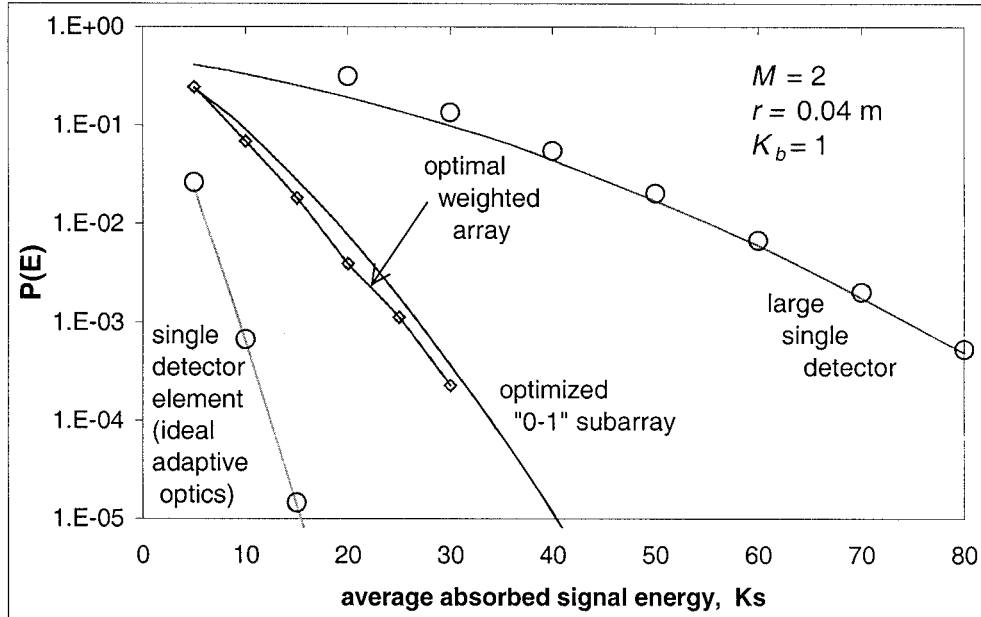


Figure 4a. Binary error probabilities: $K_b = 1$ photon/detector/slot.

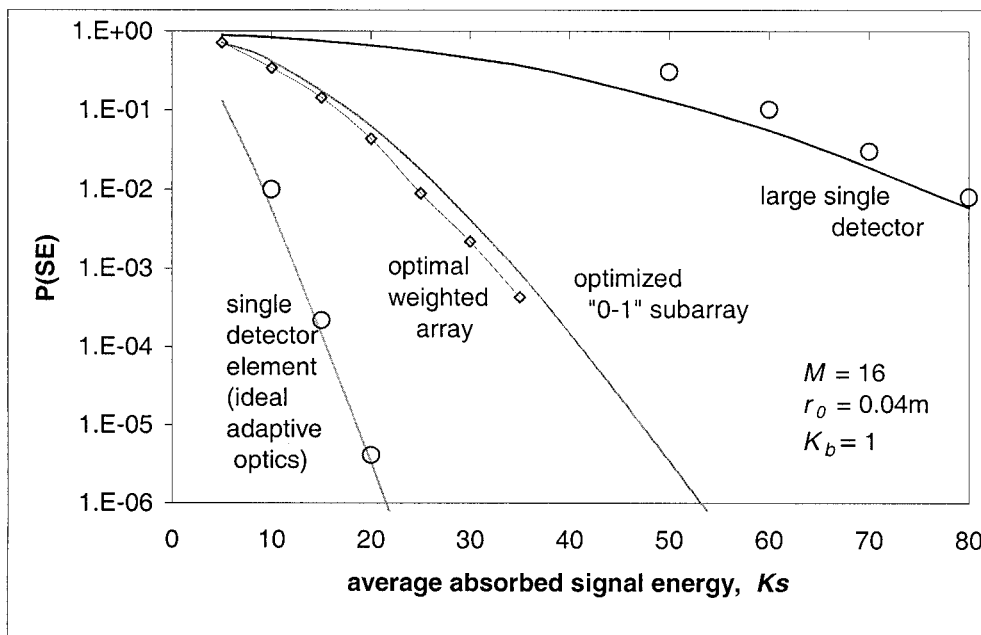


Figure 4b. Receiver performance for $M = 16$, $K_b = 1$ photon/detector/slot.

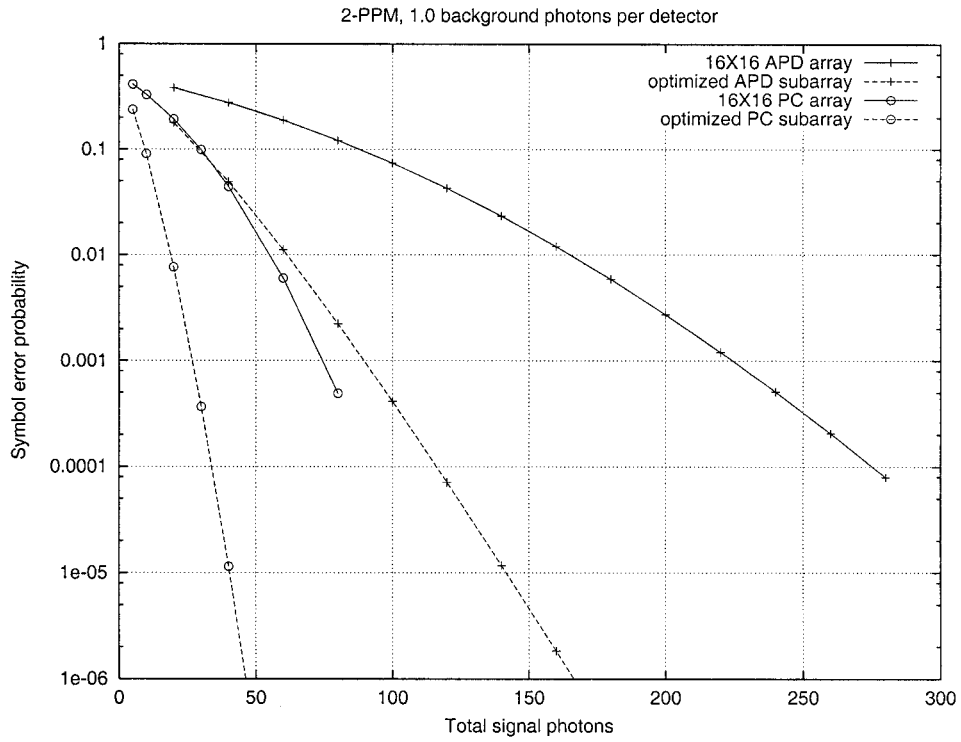


Figure 5a. APD detector array performance for $M = 2$, $K_b = 1$ photon/detector/slot.

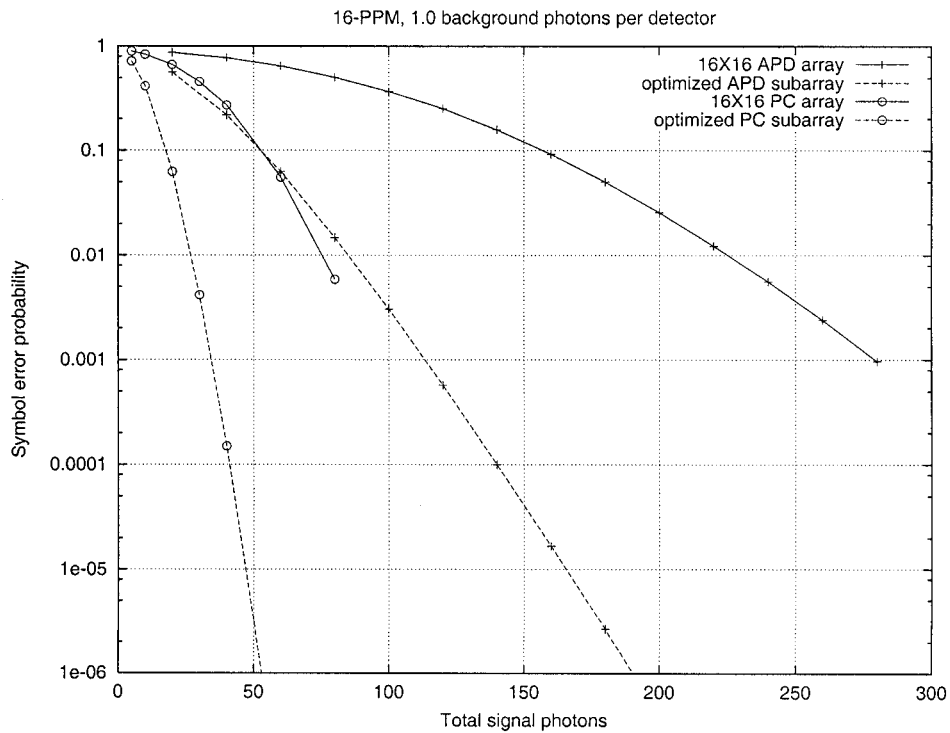


Figure 5b. APD detector array performance for $M = 16$, $K_b = 1$ photon/detector/slot.

4. SUMMARY AND CONCLUSIONS

The problem of improving the performance of ground-based optical receivers through the use of photon-counting detector arrays together with optimum signal processing algorithms has been addressed. The optimum array detection algorithm was derived, and a simpler suboptimum structure based on the optimum algorithm was also defined. Exact and approximate expressions for the error-probability performance of these structures were derived, and simulations were carried out to verify the analytic performance calculations. Realistic sample-functions of turbulence-degraded focal-plane signal distributions were generated using the Kolmogorov phase-screen algorithms described in [8], corresponding to moderate daytime turbulence (coherence-length of 4 cm), and used to evaluate the performance of optimum and suboptimum array detection algorithms designed for PPM signals. Performance improvements of nearly 5 dB were demonstrated over a single "large" detector designed to collect most of the turbulent signal, when operating in the presence of moderate to strong background radiation. The use of "ideal adaptive optics" in front of the detector which concentrates most of the signal energy into a single detector element was evaluated, and found to provide over 3 dB of additional improvement at an error probability of 0.001. It was also shown that in cases of interest, the simpler suboptimum detector array algorithm performs nearly as well as the optimal array, with considerable savings in computational complexity. Finally, the suboptimal detector array algorithm was also evaluated for APD detectors, yielding a 4 dB gain over the more conventional single APD detector matched to the signal distribution in the focal-plane, but was found to fall short of photon-counting array performance by 5.5 dB.

5. REFERENCES

1. Andrews, L.C. and Phillips, R.L., *Laser Beam Propagation through Random Media*, SPIE Optical Engineering Press, Bellingham, Washington, 1998.
2. Gagliardi, R.M. and Karp, S., *Optical Communications*, John Wiley & Sons, New York, 1976.
3. Snyder, D.L., *Random Point Processes*, John Wiley & Sons, New York, 1975.
4. Vilnrotter, V. and Srinivasan, M., "Adaptive Detector Arrays for Optical Communications Receivers," Jet Propulsion Laboratory, TMO Progress Report 42-141, May 15, 2000.
5. Papoulis, A., *Probability, Random Variables and Stochastic Processes*, McGraw-Hill, New York, 1965.
6. Hubbard, W.M., "Binary Detection in an Optical Twin Channel Receiver," IEEE Transactions on Communications Technology, vol. 19, pp. 221-223, April 1971.
7. Vilnrotter, V.A., "Optical Receivers Using Rough Reflectors," JPL Publication 85-25, May 1, 1985.
8. Negrete-Regagnon, P., "Practical aspects of image recovery by means of the bispectrum," Journal of the Optical Society of America, vol. 13, no. 7, July 1996.
9. Davidson, F. M., and Sun, S., "Gaussian approximation versus nearly exact performance analysis of optical communications systems with PPM signaling and APD receivers", IEEE Transactions on Communications, vol. COM-36, pp. 1185-1192, November 1988.
10. Srinivasan, M. and Vilnrotter, V. "Avalanche Photodiode Arrays for Optical Communications Receivers," Jet Propulsion Laboratory, TMO Progress Report 42-144, February 15, 2001.